

Flatbands and Perfect Metal in Trilayer Moiré Graphene

Christophe Mora,¹ Nicolas Regnault,¹ and B. Andrei Bernevig²

¹*Laboratoire de Physique de l'Ecole Normale Supérieure, ENS, Université PSL, CNRS, Sorbonne Université, Université Paris-Diderot, Sorbonne Paris Cité, Paris 75005, France*

²*Department of Physics, Princeton University, Princeton, New Jersey 08544, USA*

 (Received 29 January 2019; published 11 July 2019)

We investigate the electronic structure of a twisted multilayer graphene system forming a moiré pattern. We consider small twist angles separating the graphene sheets and develop a low-energy theory to describe the coupling of Dirac Bloch states close to the K point in each individual plane. Extending beyond the bilayer case, we show that, when the ratio of the consecutive twist angles is rational, a periodicity emerges in quasimomentum space with moiré Bloch bands even when the system does not exhibit a crystalline lattice structure in real space. For a trilayer geometry, we find flatbands in the spectrum at certain rotation angles. Performing a symmetry analysis of the band model for the trilayer, we prove that the system is a perfect metal in the sense that it is gapless at all energies. This striking result originates from the three Dirac cones which can only gap in pairs and produce bands with an infinite connectivity. It also holds quite generally for multilayer graphene with an odd number of planes under the condition of $C_{2z}T$ symmetry.

DOI: [10.1103/PhysRevLett.123.026402](https://doi.org/10.1103/PhysRevLett.123.026402)

Two parallel layers of graphene twisted by a small angle exhibit a moiré pattern [1], with a lattice periodicity much larger than the graphene unit cell, and nontrivial electronic properties [2], such as band flattening at certain *magic* angles [3–8]. Flatbands present a reduced kinetic energy, thereby artificially boosting electron correlations [9]. The recent discovery of correlated insulating phases at half filling and possibly unconventional superconductivity [10–13] has unveiled bilayer moiré graphene as a tunable device for exploring novel correlated states, at zero or finite magnetic field, spurring intense theoretical work in this direction [14–35]. On the other hand, moiré bands were also investigated for their topological properties [36–42], and topological phase transitions were identified close to the magic angles [39,43].

In view of the great wealth of correlation and topological phenomena occurring with moiré bilayer graphene, it is desirable to extend studies to multilayer, and specifically trilayer, geometries in which moiré patterns also appear for small rotation angles. Flatbands in bilayer result from an interplay between the K (or K') Dirac points in each layer and the situation with three or more Dirac points has yet to be explored. At low energy and close to half filling, the band structure is formed only from the electron states of the Dirac cones in each layer [44]. A moiré band theory describing such a state, that does not require a crystalline lattice, is built in Ref. [3]. In this Letter, we extend this theory to multilayer graphene and discuss in depth the symmetry and topology for three layers. We find magic angles of vanishing Dirac velocities; they are not related to a complete flattening of the spectrum, rather by a flattening

along certain symmetry lines. We also characterize the different moiré bands by the irreducible representations they generate at the high-symmetry points and lines. Based on the compatibility between these representations [45,46], we are able to prove the remarkable result that all bands are connected such that no subset of bands can be energetically isolated from the others. The most obvious consequence is that the system remains metallic at arbitrary energy. This property requires particle-hole (p - h) symmetry—neglecting the band curvature in the vicinity of the original K points. Nonetheless, slightly breaking this symmetry does not open a gap [47].

Bloch band coupling.—We detail the derivation of the band structure of the moiré pattern in twisted multilayer graphene. When the twisting angle is small, a moiré pattern is formed by the interference of lattices between the different layers. Restricting the analysis to Dirac fields near the K points of each layer [3,7,44] (see also Ref. [49]) and assuming a local short-range tunnel amplitude between atoms in consecutive planes, one derives the following Hamiltonian:

$$H^{(ab)}(\delta\mathbf{p}_a, \delta\mathbf{p}_b) = v_F \delta\mathbf{p} \cdot \boldsymbol{\sigma} \delta_{a,b} + w^{ab} \sum_{j=1}^3 \delta_{\delta\mathbf{p}_a, \delta\mathbf{p}_b + \mathbf{q}_j^{a,b}} T^j, \quad (1)$$

where w^{ab} are hopping energies between the neighboring layers a and b . The first term in Eq. (1) represents the Dirac cones in each layer and $\delta\mathbf{p}$ is a small momentum deviation from the K point for the layer a . We have introduced the matrices

$$T^{j+1} = \sigma_0 + \cos(2\pi j/3)\sigma_x + \sin(2\pi j/3)\sigma_y \quad (2)$$

associated with the three symmetric momentum directions $\mathbf{q}_1^{a,b} = M_{ab}\mathbf{K} - \mathbf{K}$, $\mathbf{q}_2^{a,b} = C_{3z}\mathbf{q}_1^{a,b}$, $\mathbf{q}_3^{a,b} = C_{3z}\mathbf{q}_2^{a,b}$. M_{ab} is the rotation around z with the twist angle θ_{ab} separating the layers a and b and C_{3z} with angle $2\pi/3$. For small twist angles, $\mathbf{q}_1^{a,b}$ is perpendicular to \mathbf{K} so that all the \mathbf{q}_j^{ab} are parallel for fixed j (see below).

The magnitudes of the vectors $|\mathbf{q}_j^{a,b}| = 2|\mathbf{K}|\sin(\theta_{ab}/2)$ depend on the twist angles. The second term in Eq. (1) couples momenta $\delta\mathbf{p}_a$ and $\delta\mathbf{p}_b + \mathbf{q}_j^{a,b}$ in layers a and b which generates a lattice in momentum space for each pair of consecutive layers. To make the calculation tractable and maintain an emergent periodicity in momentum space regardless of whether the multilayer system itself is crystalline, one has to assume that the ratios of twist angles are rational numbers. This periodicity results in moiré bands which we compute numerically and classify according to their irreducible representations at the high-symmetry points and lines. On the contrary, if the twist angles were incommensurate, or the \mathbf{q}_j^{ab} vectors are not parallel for fixed j , then successive applications of the Hamiltonian Eq. (1) would reach arbitrary momentum and the moiré periodicity would be absent.

The Hamiltonian Eq. (1) reduces to the model of Ref. [3] for bilayer and we henceforth focus on the trilayer geometry. We take the rotation angle θ_{12} as a reference and introduce the moiré magnitude $k_D = 2|\mathbf{K}|\sin(\theta_{12}/2)$. We rescale all momenta by k_D and the Hamiltonian as $\tilde{H} = H/(v_F k_D)$. Fixing the direction of $\mathbf{q}_1^{a,b}$ along y , we use the complex notation

$$q_1^{23} = e^{i(\pi/2)}, \quad q_2^{23} = e^{i(7\pi/6)}, \quad q_3^{23} = e^{-i(\pi/6)}, \quad (3)$$

and $q_j^{12} = (p/q)q_j^{23}$ for all j , where p and q are coprime integers. The Hamiltonian Eq. (1) can then be written as

$$\tilde{H}_{Q_m Q_n}(k) = (\mathbf{k} - \mathbf{Q}_m) \cdot \boldsymbol{\sigma} \delta_{mn} + \alpha \sum_j T^j \delta_{Q_m, Q_n - q_j^{mn}}, \quad (4)$$

where we assume a uniform tunnel amplitude $w_{ab} = w$ and introduce the dimensionless coupling $\alpha = w/(v_F k_D)$ between Dirac cones. The vectors \mathbf{Q}_m form a k -space lattice, see Fig. 1(b), where each site is associated to a specific layer.

Equal twist angles.—We first consider the most symmetric case of evenly rotated planes where $q_j^{12} = q_j^{23}$. A representative set of moiré spectra obtained from Eq. (4) with different values of the coupling α is displayed in Figs. 2(a)–2(d). The moiré bands exhibit a rich structure. The first remarkable feature is that all bands are connected: it is impossible to isolate a set of bands that are detached from the rest. We provide below a formal proof for this statement based on irreducible representations at symmetric

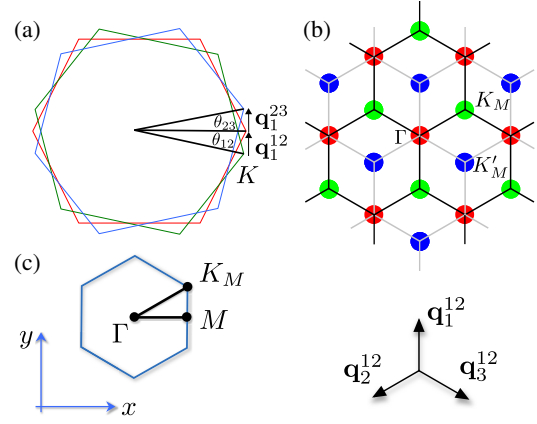


FIG. 1. Trilayer graphene with the same rotation angle $\theta_{12} = \theta_{23}$ between consecutive layers. (a) Original Brillouin zones in each layer with their respective K points. (b) k -space lattice generated by the vectors \mathbf{q}_j^{ab} (for $\mathbf{q}_j^{12} = \mathbf{q}_j^{23}$). Green, red, and blue sites belong, respectively, to the layers 1,2,3. (c) Moiré Brillouin zone with high-symmetry points Γ , K_M , K'_M , M and high-symmetry lines (in black).

points and lines, and afterwards extend it to arbitrary p and q .

Three Dirac cones are attached at zero energy to the points Γ , K_M , and K'_M [see Fig. 1(b)] as α is varied. We display the corresponding Dirac velocities of the cones at Γ and K_M (with K'_M velocity linked by symmetry to that of K_M) in Fig. 2(e) and find a set of *magic angles*—in analogy with the bilayer case—where one of these velocities vanishes. The difference with the bilayer case is that these magic angles are not associated with a flattening of the whole spectrum which would be at odds with the fully connected band structure. However, we do see a flattening of part of the spectrum close to magic angles: on the $M - K_M$ line (for the second levels) when $\alpha = 0.28$, close to Γ when $\alpha = 0.85$, for the first two magic angles. This flattening along one-dimensional directions in k space opens interesting perspectives for the realization of exotic correlated many-body physics. Of course the property of a gapless spectrum cannot result in a quenched kinetic energy as occurs in the bilayer case [3–8]. However, tuning the chemical potential close to flat regions of the spectrum increases strongly the density of states and is likely to lead to instabilities towards charge-ordered or superconducting anisotropic phases [50,51].

Symmetries.—The moiré reciprocal lattice vectors $b_1 = q_1^{12} - q_2^{12}$, $b_2 = q_1^{12} - q_3^{12}$ generate the whole lattice in Fig. 1(b). The different layers (colors) are coupled by the $\mathbf{q}_j^{a,b}$ vectors. Bloch periodicity takes the form

$$\tilde{H}(k - b_i) = V^{b_i} \tilde{H}(k) V^{b_i \dagger}, \quad V_{Q_m, Q_n}^{b_i} = \delta_{Q_n, Q_m + b_i}. \quad (5)$$

The spectrum is thus invariant upon shifting the origin of k by a combination of b_1 and b_2 .

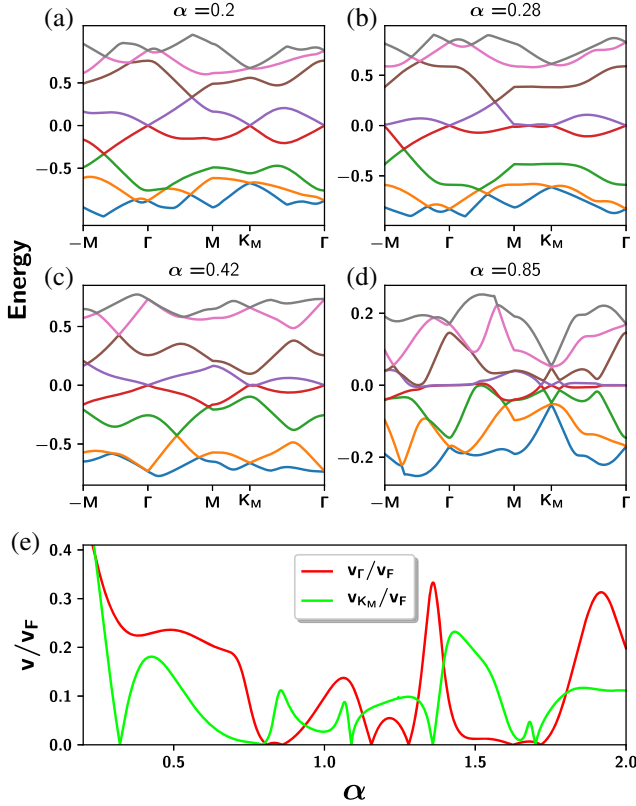


FIG. 2. Moiré bands (a)–(d) and renormalized Dirac-point velocities (e) at the symmetric points Γ (red line) and K_M (green line). The eight bands closest to zero energy are represented along the moiré Brillouin zone trajectory $-M \rightarrow \Gamma \rightarrow M \rightarrow K_M \rightarrow \Gamma$ for $\alpha = 0.2, 0.28, 0.42, 0.85$ (a)–(d). The particle-hole symmetry discussed in the main text—sending k to $-k$ and E to $-E$ —is clearly visible along the path $-M \rightarrow \Gamma \rightarrow M$. (e) Velocities of the two Dirac cones at Γ and K_M as function of α .

The moiré lattice also transforms into itself by the action of a $2\pi/3$ rotation C_{3z} around Γ . In the Hamiltonian language, the corresponding operator is given by $C_{3z} = \exp(i2\pi\sigma_z/3)\delta_{Q_m, C_{3z}Q_n}$. We note that if Q_n is in a given layer, so is $C_{3z}Q_n$, such that the three layers are not mixed by the rotation. The C_{2x} symmetry operates a reflection across the x axis going through the Γ point [red dot in Fig. 1(b)]. As such, C_{2x} sends lattice sites of layer 1 to 3 and vice versa but keeps layer 2 invariant. The corresponding symmetry operator is $C_{2x} = \sigma_x \delta_{Q_m, C_{2x}Q_n}$. The two symmetry operators induce the Hamiltonian transformation,

$$C_{3z}\tilde{H}(k)C_{3z}^\dagger = \tilde{H}(C_{3z}k), \quad C_{2x}\tilde{H}(k)C_{2x}^\dagger = \tilde{H}(C_{2x}k), \quad (6)$$

which leave the spectrum invariant. The antiunitary $C_{2z}\mathcal{T}$ symmetry acts locally on the moiré lattice. It takes complex conjugation K and reverses the pseudospin direction. It is represented by the operator $C_{2z}\mathcal{T} = \sigma_x \delta_{Q_m, Q_n} K$, which

squares to 1 and commutes with the Hamiltonian $\tilde{H}(k)$. It also commutes with the spatial symmetries C_{3z} and C_{2x} .

The moiré model also possesses a unitary particle-hole symmetry. The original $k \cdot p$ Dirac Hamiltonian of the single layer graphene sheet $H(k) = \vec{k} \cdot \vec{\sigma}$ has a unitary particle-hole symmetry $H(k) = -H(-k)$ due to the absence of k^2 terms in the Hamiltonian. Since our model is based on this low-energy expansion, it retains a similar symmetry with the operator

$$\mathcal{P} = \delta_{Q_m, -Q_n} \zeta_{Q_n}, \quad (7)$$

where ζ_{Q_n} is $+1$ for Q_n belonging to the lower and top layers and -1 for the middle layer. With this, we have $\mathcal{P}^2 = \mathcal{P}\mathcal{P}^\dagger = 1$. Importantly, one checks that \mathcal{P} commutes with all other symmetry operators, C_{3z} , C_{2x} and $C_{2z}\mathcal{T}$, and satisfies

$$\mathcal{P}\tilde{H}(k)\mathcal{P}^\dagger = -\tilde{H}(-k). \quad (8)$$

This is to be contrasted with the p - h operator \mathcal{P}_{bi} identified [39] for moiré bilayer which has (i) $\mathcal{P}_{\text{bi}}^2 = 1$ and (ii) anti-commutes with C_{2x} , i.e., $\{\mathcal{P}_{\text{bi}}, C_{2x}\} = 0$, instead of the commutation found for \mathcal{P} .

Based on the generators discussed so far, the symmetry group of the moiré lattice is the magnetic space group called $P6'2'2$ (no. 177.151 in the BNS notation [52]). Although the same group describes moiré bilayer, the physics is different here. It indeed originates from three Dirac cones, instead of two, and the extra particle-hole symmetry is essentially different. The high-symmetry points and their little cogroups are Γ ($C_{2x}, C_{3z}, C_{2z}\mathcal{T}, \mathcal{P}$), K_M ($C_{3z}, C_{2z}\mathcal{T}, \mathcal{P}C_{2x}$), and M ($C_{2x}, C_{2z}\mathcal{T}, \mathcal{P}$). The symmetries on the high-symmetry lines are $\Gamma - M$ ($C_{2x}, C_{2z}\mathcal{T}$) and $\Gamma - K_M$ ($C_{2x}\mathcal{P}, C_{2z}\mathcal{T}$). The classification of the different irreducible representations at the symmetric points and lines are given in Table I. At Γ , M , K_M and on the line $\Gamma - M$, each energy or band in Fig. 2 is characterized by a certain representation determined from the character, i.e., from the eigenvalues of the operators C_{3z} and C_{2x} restricted to this (possibly degenerate) energy.

First proof of all-connected bands.—We now prove by contradiction that all bands are connected such that there is

TABLE I. Character table of irreducible representations at high-symmetry momenta and lines in magnetic space group $P6'2'2$. E , C_3 , and C_2 represent the conjugation classes generated from identity, C_{3z} and C_{2x} . The notation ΓM_i stands for the symmetric line $\Gamma - M$.

	Γ_1	Γ_2	Γ_3		M_1	M_2		K_1	K_2	K_3		ΓM_1	ΓM_2
E	1	1	2	E	1	1	E	1	2	E	1	1	1
$2C_3$	1	1	-1	C_2	1	-1	C_3	1	-1	C_2	1	-1	-1
$3C_2$	1	-1	0				C_3^{-1}	1	-1				

no gap in the spectrum at any energy. We assume a subspace of isolated bands between the energies $\varepsilon_{1,k}$ and $\varepsilon_{2,k}$. By p - h symmetry, a symmetric set of bands exists in the energy window $(-\varepsilon_{2,-k}, -\varepsilon_{1,-k})$ and, consequently, the N_1 bands between $-\varepsilon_{1,-k}$ and $\varepsilon_{1,k}$ must be disconnected from all other bands. We focus on these N_1 bands and investigate their transformation property under \mathcal{C}_{2x} . \mathcal{C}_{2x} remains a symmetry along the line connecting Γ and M such that their total character must coincide at each end, or $\chi_{\mathcal{C}_{2\Gamma}} = \chi_{\mathcal{C}_{2M}}$.

We call m_{Γ_i} the multiplicity of the representation $i = 1, 2, 3$ in the set of N_1 bands, and m_{M_i} the multiplicity of the representation $i = 1, 2$ in the set of N_1 bands at M . Hence we have the equations $m_{\Gamma_1} + m_{\Gamma_2} + 2m_{\Gamma_3} = N_1$, $m_{M_1} + m_{M_2} = N_1$, $m_{\Gamma_1} - m_{\Gamma_2} = \chi_{\mathcal{C}_{2\Gamma}}$, and $m_{M_1} - m_{M_2} = \chi_{\mathcal{C}_{2M}}$, which leads to

$$m_{M_2} = m_{\Gamma_2} + m_{\Gamma_3}. \quad (9)$$

For $\alpha = 0$, we have three Dirac cones around Γ , K_M , and K'_M and a gapped spectrum at M . At Γ , the zero-energy subspace is doubly degenerate and the character of \mathcal{C}_{3z} is simply given by $\text{Tr}(e^{i(2\pi/3)\sigma_z}) = -1$ corresponding to the irreducible representation Γ_3 as indicated in Table I. We thus have $m_{\Gamma_3} = 1$, $m_{M_2} = m_{\Gamma_2} = 0$ when restricted to zero energy and $\alpha = 0$. Increasing α away from zero, the \mathcal{P} symmetry is maintained and commutes with \mathcal{C}_{3z} and \mathcal{C}_{2x} such that any band associated to a given representation collapsing at (or departing from) zero energy, at either Γ or M , must move with its energy symmetric p - h partner associated to the same representation. As a result, the multiplicities m_{Γ_j} and m_{M_j} can only change by units of two in such processes. The same argument extends to nonzero energies where each band with energy ε and representation Γ_j (or M_j) has a p - h partner with energy $-\varepsilon$ and the same representation. Since k and $-k$ are identified at Γ and M such that the interval $(-\varepsilon_{1,-k}, +\varepsilon_{1,k})$ is symmetric, we finally obtain by continuity with α that the multiplicity m_{Γ_3} must be odd while m_{M_2} and m_{Γ_2} are both even integers. It contradicts Eq. (9), thus completing the proof.

General proof for unequal twist angles.—Our discussion has so far been restricted to the symmetric configuration of equal p and q . The \mathcal{C}_{2x} and \mathcal{P} symmetries are broken when p and q are different whereas \mathcal{C}_{3z} and $\mathcal{C}_{2z}\mathcal{T}$ are maintained. However, a remnant of p - h symmetry still exists in the form of a mirror symmetry $\Pi_{\pi/6}$ with respect to the plane orthogonal to the layer and crossing Γ and K_M , leaving each layer invariant. It corresponds to the operator $\Pi_{\pi/6} = \mathcal{P}\mathcal{C}_{2x}\mathcal{C}_{3z}$, with $\Pi_{\pi/6}^2 = 1$, acting as

$$\Pi_{\pi/6}\tilde{H}(k)\Pi_{\pi/6}^\dagger = -\tilde{H}(\Pi_{\pi/6}k), \quad (10)$$

which associates pairs of mirror-symmetric momenta with opposite energies. Extending the arguments of Ref. [40], we show that a set of isolated bands with $\mathcal{C}_{2z}\mathcal{T}$ symmetry

cannot accommodate an odd winding number N_t , corresponding, e.g., to an odd number of Dirac cones. The derivation is explicit in Refs. [39,40] for two bands and a vanishing total Berry phase (Wilson loop) with $N_t = -2e_2$, where the Euler class e_2 is an integer topological invariant. Adding more bands, windings around singularities can change sign but keep a definite parity while the parity of e_2 defines a \mathbb{Z}_2 topological invariant, the Stiefel-Whitney class w_2 . Then, the relation $N_t = -2w_2$ simply enforces that the winding number must be an even integer. More intuitively, we note that Dirac points are monopoles attaching Dirac strings. They can annihilate in pairs when of opposite signs or form a topological isolated band by combining pairs of the same sign [38,39], but in all cases they need to pair to form an isolated set of bands.

We now show by contradiction that all bands are connected by gapless points in our trilayer moiré model for arbitrary p and q . As already discussed above, we can assume, without loss of generality, a set of disconnected bands symmetric around zero energy. Particle-hole symmetry implies that all band crossings at nonzero energy come in pairs, such that the analysis of the parity of N_t can be restricted to zero-energy modes. A single Dirac cone is protected by $\mathcal{C}_{2z}\mathcal{T}$ and is pinned at zero energy by p - h symmetry. Particle-hole symmetry further protects the parity of N_t for zero modes as α is varied. By continuity with the case $\alpha = 0$, where we have three Dirac cones and $N_t = 3$, we finally obtain that N_t is odd, in contradiction with $N_t = -2w_2$, which completes our proof that all bands must be connected.

In summary, we showed that trilayer twisted graphene exhibits band flattening along symmetry lines and close to magic angles. We also proved, by compatibility of band representations for evenly twisted planes or by counting an odd number of Dirac points protected by $\mathcal{C}_{2z}\mathcal{T}$, that the system is always a metal with an infinite connectivity, an unprecedented feature in standard materials [45,53–55]. This property relies on p - h symmetry emerging for small twisting angles. We checked that this condition is practically realized already for angles close to the first magic angle [47]. Since it originates from the underlying three Dirac cones, we conjecture that the property of infinite band connectivity will appear in many other configurations, such as multilayer moiré graphene with an odd number of planes. To further test this conjecture, we computed the band spectrum [47] for four and five twisted layers with indeed the result that it is fully connected for five but not for four layers.

We would like to thank B. Estienne and Biao Lian for fruitful discussions. B. A. B. is supported by the Department of Energy Grant No. de-sc0016239, the National Science Foundation EAGER Grant No. noaawd1004957, Simons Investigator Grants No. ONRN00014-14-1-0330, No. ARO MURI W911NF-12-1-0461, and No. NSF-MRSEC DMR-1420541, the Packard Foundation, and the Schmidt Fund for Innovative Research.

- [1] W.-T. Pong and C. Durkan, A review and outlook for an anomaly of scanning tunnelling microscopy (STM): Superlattices on graphite, *J. Phys. D* **38**, R329 (2005).
- [2] R. Bistritzer and A. H. MacDonald, Transport between twisted graphene layers, *Phys. Rev. B* **81**, 245412 (2010).
- [3] R. Bistritzer and A. H. MacDonald, Moiré bands in twisted double-layer graphene, *Proc. Natl. Acad. Sci. U.S.A.* **108**, 12233 (2011).
- [4] G. Trambly de Laissardière, D. Mayou, and L. Magaud, Localization of dirac electrons in rotated graphene bilayers, *Nano Lett.* **10**, 804 (2010).
- [5] P. San-Jose, J. González, and F. Guinea, Non-Abelian Gauge Potentials in Graphene Bilayers, *Phys. Rev. Lett.* **108**, 216802 (2012).
- [6] J. M. B. Lopes dos Santos, N. M. R. Peres, and A. H. Castro Neto, Continuum model of the twisted graphene bilayer, *Phys. Rev. B* **86**, 155449 (2012).
- [7] S. Fang and E. Kaxiras, Electronic structure theory of weakly interacting bilayers, *Phys. Rev. B* **93**, 235153 (2016).
- [8] G. Tarnopolsky, A. J. Kruchkov, and A. Vishwanath, Origin of Magic Angles in Twisted Bilayer Graphene, *Phys. Rev. Lett.* **122**, 106405 (2019).
- [9] K. Kim, A. DaSilva, S. Huang, B. Fallahazad, S. Larentis, T. Taniguchi, K. Watanabe, B. J. LeRoy, A. H. MacDonald, and E. Tutuc, Tunable moiré bands and strong correlations in small-twist-angle bilayer graphene, *Proc. Natl. Acad. Sci. U.S.A.* **114**, 3364 (2017).
- [10] Y. Cao, V. Fatemi, A. Demir, S. Fang, S. L. Tomarken, J. Y. Luo, J. D. Sanchez-Yamagishi, K. Watanabe, T. Taniguchi, E. Kaxiras *et al.*, Correlated insulator behaviour at half-filling in magic-angle graphene superlattices, *Nature (London)* **556**, 80 (2018).
- [11] Y. Cao, V. Fatemi, S. Fang, K. Watanabe, T. Taniguchi, E. Kaxiras, and P. Jarillo-Herrero, Unconventional superconductivity in magic-angle graphene superlattices, *Nature (London)* **556**, 43 (2018).
- [12] S. Carr, S. Fang, P. Jarillo-Herrero, and E. Kaxiras, Pressure dependence of the magic twist angle in graphene superlattices, *Phys. Rev. B* **98**, 085144 (2018).
- [13] M. Yankowitz, S. Chen, H. Polshyn, K. Watanabe, T. Taniguchi, D. Graf, A. F. Young, and C. R. Dean, Tuning superconductivity in twisted bilayer graphene, *Science* **363**, 1059 (2019).
- [14] N. F. Q. Yuan and L. Fu, Model for the metal-insulator transition in graphene superlattices and beyond, *Phys. Rev. B* **98**, 045103 (2018).
- [15] F. Wu, A. H. MacDonald, and I. Martin, Theory of Phonon-Mediated Superconductivity in Twisted Bilayer Graphene, *Phys. Rev. Lett.* **121**, 257001 (2018).
- [16] B. Padhi, C. Setty, and P. W. Phillips, Doped twisted bilayer graphene near magic angles: Proximity to Wigner crystallization, not Mott insulation, *Nano Lett.* **18**, 6175 (2018).
- [17] H. C. Po, L. Zou, A. Vishwanath, and T. Senthil, Origin of Mott Insulating Behavior and Superconductivity in Twisted Bilayer Graphene, *Phys. Rev. X* **8**, 031089 (2018).
- [18] H. Isobe, N. F. Q. Yuan, and L. Fu, Unconventional Superconductivity and Density Waves in Twisted Bilayer Graphene, *Phys. Rev. X* **8**, 041041 (2018).
- [19] J. F. Dodaro, S. A. Kivelson, Y. Schattner, X. Q. Sun, and C. Wang, Phases of a phenomenological model of twisted bilayer graphene, *Phys. Rev. B* **98**, 075154 (2018).
- [20] G. Baskaran, Theory of emergent Josephson lattice in neutral twisted bilayer graphene (moiré is different), [arXiv:1804.00627](https://arxiv.org/abs/1804.00627).
- [21] T. Huang, L. Zhang, and T. Ma, Antiferromagnetically ordered Mott insulator and $d + id$ superconductivity in twisted bilayer graphene: A quantum Monte Carlo study, *Sci. Bull.* **64**, 310 (2019).
- [22] Y.-Z. You and A. Vishwanath, Superconductivity from valley fluctuations and approximate SO(4) symmetry in a weak coupling theory of twisted bilayer graphene, [arXiv:1805.06867](https://arxiv.org/abs/1805.06867).
- [23] X.-C. Wu, K. A. Pawlak, C.-M. Jian, and C. Xu, Emergent Superconductivity in the weak Mott insulator phase of bilayer graphene moiré superlattice, [arXiv:1805.06906](https://arxiv.org/abs/1805.06906).
- [24] B. Roy and V. Juricic, Unconventional superconductivity in nearly flat bands in twisted bilayer graphene, *Phys. Rev. B* **99**, 121407 (2019).
- [25] C. Xu and L. Balents, Topological Superconductivity in Twisted Multilayer Graphene, *Phys. Rev. Lett.* **121**, 087001 (2018).
- [26] Y.-H. Zhang, D. Mao, Y. Cao, P. Jarillo-Herrero, and T. Senthil, Moiré superlattice with nearly flat Chern bands: Platform for (fractional) quantum anomalous Hall effects and unconventional superconductivity, *Phys. Rev. B* **99**, 075127 (2019).
- [27] M. Koshino, N. F. Q. Yuan, T. Koretsune, M. Ochi, K. Kuroki, and L. Fu, Maximally Localized Wannier Orbitals and the Extended Hubbard Model for Twisted Bilayer Graphene, *Phys. Rev. X* **8**, 031087 (2018).
- [28] J. Kang and O. Vafek, Symmetry, Maximally Localized Wannier States, and a Low-Energy Model for Twisted Bilayer Graphene Narrow Bands, *Phys. Rev. X* **8**, 031088 (2018).
- [29] S. Ray and T. Das, Wannier pairs in the superconducting twisted bilayer graphene and related systems, *Phys. Rev. B* **99**, 134515 (2019).
- [30] F. Guinea and N. R. Walet, Electrostatic effects and band distortions in twisted graphene bilayers, *Proc. Natl. Acad. Sci. U.S.A.* **115**, 13174 (2018).
- [31] B. Lian, Z. Wang, and B. A. Bernevig, Twisted bilayer graphene: A phonon driven superconductor, [arXiv:1807.04382](https://arxiv.org/abs/1807.04382) [*Phys. Rev. Lett.* (to be published)].
- [32] J. Kang and O. Vafek, Strong coupling phases of partially filled twisted bilayer graphene narrow bands, [arXiv:1810.08642](https://arxiv.org/abs/1810.08642) [*Phys. Rev. Lett.* (to be published)].
- [33] B. Lian, F. Xie, and B. A. Bernevig, The Landau level of fragile topology, [arXiv:1811.11786](https://arxiv.org/abs/1811.11786).
- [34] A. Ramires and J. L. Lado, Electrically Tunable Gauge Fields in Tiny-Angle Twisted Bilayer Graphene, *Phys. Rev. Lett.* **121**, 146801 (2018).
- [35] D. M. Kennes, J. Lischner, and C. Karrasch, Strong correlations and $d + id$ superconductivity in twisted bilayer graphene, *Phys. Rev. B* **98**, 241407(R) (2018).
- [36] P. San-Jose and E. Prada, Helical networks in twisted bilayer graphene under interlayer bias, *Phys. Rev. B* **88**, 121408(R) (2013).

- [37] R. de Gail, M. O. Goerbig, F. Guinea, G. Montambaux, and A. H. Castro Neto, Topologically protected zero modes in twisted bilayer graphene, *Phys. Rev. B* **84**, 045436 (2011).
- [38] H. C. Po, L. Zou, T. Senthil, and A. Vishwanath, Faithful tight-binding models and fragile topology of magic-angle bilayer graphene, *Phys. Rev. B* **99**, 195455 (2019).
- [39] Z. Song, Z. Wang, W. Shi, G. Li, C. Fang, and B. A. Bernevig, “Magic angles” are “stable” topological, [arXiv:1807.10676](https://arxiv.org/abs/1807.10676) [Phys. Rev. Lett. (to be published)].
- [40] J. Ahn, S. Park, and B.-J. Yang, Failure of Nielsen-Ninomiya Theorem and Fragile Topology in Two-Dimensional Systems with Space-Time Inversion Symmetry: Application to Twisted Bilayer Graphene at Magic Angle, *Phys. Rev. X* **9**, 021013 (2019).
- [41] L. Zou, H. C. Po, A. Vishwanath, and T. Senthil, Band structure of twisted bilayer graphene: Emergent symmetries, commensurate approximants, and Wannier obstructions, *Phys. Rev. B* **98**, 085435 (2018).
- [42] J. Liu, J. Liu, and X. Dai, A complete picture for the band topology in twisted bilayer graphene, *Phys. Rev. B* **99**, 155415 (2019).
- [43] K. Hejazi, C. Liu, H. Shapourian, X. Chen, and L. Balents, Multiple topological transitions in twisted bilayer graphene near the first magic angle, *Phys. Rev. B* **99**, 035111 (2019).
- [44] J. M. B. Lopes dos Santos, N. M. R. Peres, and A. H. Castro Neto, Graphene Bilayer with a Twist: Electronic Structure, *Phys. Rev. Lett.* **99**, 256802 (2007).
- [45] B. Bradlyn, L. Elcoro, J. Cano, M. G. Vergniory, Z. Wang, C. Felser, M. I. Aroyo, and B. Andrei Bernevig, Topological quantum chemistry, *Nature (London)* **547**, 298 (2017).
- [46] M. G. Vergniory, L. Elcoro, Z. Wang, J. Cano, C. Felser, M. I. Aroyo, B. A. Bernevig, and B. Bradlyn, Graph theory data for topological quantum chemistry, *Phys. Rev. E* **96**, 023310 (2017).
- [47] See Supplemental Material at <http://link.aps.org/supplemental/10.1103/PhysRevLett.123.026402> for the numerical investigation of p - h symmetry breaking, more details on the symmetries, the positions of the Dirac points at $\alpha = 0$, local density of states, and band spectra for four and five twisted layers, which also includes Refs. [4,6,7,48].
- [48] Y. Cao, J. Y. Luo, V. Fatemi, S. Fang, J. D. Sanchez-Yamagishi, K. Watanabe, T. Taniguchi, E. Kaxiras, and P. Jarillo-Herrero, Superlattice-Induced Insulating States and Valley-Protected Orbits in Twisted Bilayer Graphene, *Phys. Rev. Lett.* **117**, 116804 (2016).
- [49] B. Amorim and E. V. Castro, Electronic spectral properties of incommensurate twisted trilayer graphene, [arXiv:1807.11909](https://arxiv.org/abs/1807.11909).
- [50] Y. Sherkunov and J. J. Betouras, Electronic phases in twisted bilayer graphene at magic angles as a result of van Hove singularities and interactions, *Phys. Rev. B* **98**, 205151 (2018).
- [51] J. González and T. Stauber, Kohn-Luttinger Superconductivity in Twisted Bilayer Graphene, *Phys. Rev. Lett.* **122**, 026801 (2019).
- [52] S. V. Gallego, E. S. Tasci, G. Flor, J. M. Perez-Mato, and M. I. Aroyo, Magnetic symmetry in the Bilbao Crystallographic Server: A computer program to provide systematic absences of magnetic neutron diffraction, *J. Appl. Crystallogr.* **45**, 1236 (2012).
- [53] M. G. Vergniory, L. Elcoro, C. Felser, B. A. Bernevig, and Z. Wang, The (high quality) topological materials in the world, *Nature (London)* **566**, 480 (2019).
- [54] T. Zhang, Y. Jiang, Z. Song, H. Huang, Y. He, Z. Fang, H. Weng, and C. Fang, Catalogue of topological electronic materials, *Nature (London)* **566**, 475 (2019).
- [55] F. Tang, H. C. Po, A. Vishwanath, and X. Wan, Towards ideal topological materials: Comprehensive database searches using symmetry indicators, *Nature (London)* **566**, 486 (2019).